Journal of the Mechanics and Physics of Solids 57 (2009) 1958–1979

Contents lists available at ScienceDirect

Journal of the Mechanics and Physics of Solids

journal homepage: www.elsevier.com/locate/jmps

Localised knife waves in a structured interface

Gennady S. Mishuris [a], Alexander B. Movchan [b,*], Leonid I. Slepyan [c]

[a] Institute of Mathematics and Physics, Aberystwyth University, UK
[b] Department of Mathematical Sciences, University of Liverpool, UK
[c] School of Mechanical Engineering, Tel Aviv University, Israel

ARTICLE INFO

Article history:
Received 28 August 2008
Received in revised form
3 August 2009
Accepted 5 August 2009

Keywords:
A. Dynamic fracture
A. Vibrations
B. Inhomogeneous material
B. Supersonic crack
C. Integral transforms

ABSTRACT

We consider a Mode III lattice with an interface layer where the dynamic crack growth is caused by a localised sinusoidal wave. In the wave–fracture scenario, the 'feeding wave' (here also called the *knife wave*) delivers energy to the moving crack front, while the dissipative waves carry a part of this energy away from the front. The questions addressed here are:

- What are the conditions of existence of the localised knife wave?
- What is the lower bound of the amplitude of the feeding wave, which supports the crack propagation, for a given deformational fracture criterion?
- How does the crack speed depend on the amplitude of the feeding wave?
- What are the dissipative waves? How much energy is irradiated by these waves and what is the total dissipation?
- What are the conditions of existence of the steady-state regime for the propagating crack?

We consider analytically two established regimes: the steady-state regime, where the motion of neighbouring masses (along the interface) differs only by a constant shift in time, and an alternating-strain regime, where the corresponding amplitudes differ by sign. We also present the numerical simulation results for a model of a high-contrast interface structure. Along with the energy of the feeding and dissipative waves, an energy radiated to the bulk of the lattice is identified.

1. Introduction

The motivation for the present work comes from the real life experiments on high-speed rupture within structural interfaces and, in particular, within regions of frictional contact. As presented in the paper by Coker et al. (2005), a high speed rupture is observed at an interface between two elastic materials, which were in frictional contact under the applied pressure and shear loading. For a homogeneous elastic material, a special value of the mode II intersonic crack speed was found, $v = c_s\sqrt{2}$, where there is no wave radiation from the propagating crack, and the crack tip asymptotes have the required square root type.

Intersonic crack propagation was considered, in particular, in Burridge (1976), Freund (1979), Slepyan and Fishkov (1981), Broberg (1999), and Gao et al. (1999). Numerical simulations and experiments also demonstrate a possibility of intersonic crack propagation—see Rosakis et al. (1998, 1999), Needleman and Rosakis (1999) and Abraham and Gao (2000).

* Corresponding author.
E-mail address: abm@liverpool.ac.uk (A.B. Movchan).

0022-5096/$ - see front matter © 2009 Elsevier Ltd. All rights reserved.
doi:10.1016/j.jmps.2009.08.004

Also see Slepyan (2002, Section 12.4.4). Marder (2006) has found that the supersonic crack propagation can occur in a nonlinear material.

On the other hand, in lattice structures, the supersonic fracture can occur under high-frequency lattice vibrations as was presented by Slepyan (1981), also see Slepyan (2002, Section 11.5.4). In this theoretical study, a uniform lattice was considered, and no localisation of waves was present, whereas for problems of structural interfaces localisation features can be anticipated. This concept is consistent with the notion of structural contact via models of lattice interfaces (see, for example, Edagawa et al., 1977; Gerde and Marder, 2001; Movchan et al., 2003). In this connection, we also note some earlier papers on dynamic fracture within inhomogeneous lattices of periodic structures, Mishuris et al. (2007, 2008a, 2008b), which include analytical representation for the displacement around the crack, dissipation rate, and issues of homogenisation approximations.

In the present work, we consider the steady-state and the 'alternating-strain steady-state' dynamic fracture caused by high-frequency exponentially localised harmonic waves.

We address a scalar model of antiplane shear of a square lattice containing an interface layer, which possesses different elastic and/or inertia properties compared to the ambient infinite lattice. We consider rupture propagating along such an interface, where the energy is supplied by a high frequency 'feeding wave', exponentially localised at the interface; here to emphasise the strong localisation we also call it the *knife wave*.

The plan of the paper is as follows. Sections 2 and 3 include the description of the geometry of the inhomogeneous lattice with the crack, governing equations for the displacements of the nodes of the lattice, and the equivalent formulation in terms of the Fourier transforms. In Section 4, we formulate and solve model problems for the lattice half planes with different types (Neumann or Dirichlet) boundary conditions on their edge. The corresponding dispersion diagrams are linked to the waves behind the crack front and waves ahead of the crack. Given the knife wave frequency the diagrams allow to determine directly the possible crack speed and also the frequencies and the group velocities of the dissipative waves.

The crack dynamics problem considered in Section 5 is reduced to the functional equation of the Wiener–Hopf type, which is solved in the closed analytical form. In Section 6, we analyse the properties of the kernel function of the main functional equation, which are closely linked to the characteristics of the knife wave, which supplies the energy to the propagating crack, and of the dissipative waves. A special alternating-strain formulation is introduced and analysed in Section 7. Results of numerical simulations, which support the analytically considered regimes of the knife-wave rupture and have revealed some 'crack-speed-oscillating' regimes, are presented in Section 8. Then in Sections 9.1 and 9.2, we consider particularly important cases of a low contrast (light) interface and of a heavy interface. A special attention is given to the analysis of the energy relations as the comparative rates of the energies of the knife wave and the dissipative waves, Section 10.

2. Formulation of the problem. Governing equations

We consider a Mode III dynamic fracture of a square lattice shown in Fig. 1. The lattice consists of point masses M_1, M_2, connected by linearly elastic bonds of stiffnesses C_1 and C_2. The masses M_1, together with the bonds of the stiffness C_1, form the structured interface. Given (m,n) as a multi-index characterising a position of a mass within the lattice, the structured interface involves two layers with $n=\pm 1$ together with the connecting bonds, whereas the bulk of the lattice lies above and below the interface, i.e. it consists of the layers $n=\pm 2, \pm 3, \ldots$. The normalisation is introduced in such a way that the lattice spacing is equal to 1. The crack is assumed to propagate between the layers $n=1$ and -1, with a constant speed v. This implies that the time interval between the breakages of neighbouring bonds is equal to $1/v$.

The loading is imposed via a high-frequency 'feeding' wave propagating in the same direction as the crack itself. In addition to this wave, there exist 'dissipative waves' excited by the propagating crack. For the structures considered below, these waves are exponentially localised in a neighbourhood of the interface, i.e. they appear to decay exponentially as $|n|\to\infty$.

Let $u_{m,n}(t)$ be the displacement of the node (m,n) at time t. Taking into account the symmetry, $u_{m,n}(t)=-u_{m,-n}(t)$, we consider only the upper half-plane as shown in Fig. 1. We note that behind the crack front there are no forces acting from below on the masses of the layer $n=1$, whereas ahead of the crack the intact bonds have zero displacement on the horizontal symmetry line.

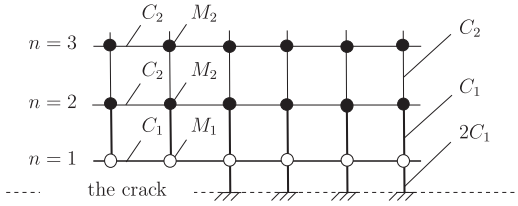

Fig. 1. The lattice with the propagating crack. The upper part of the symmetric structure is shown. The structural interface consists of two lines, $n=1$ and -1 (the latter is not shown) of masses M_1 connected with each other and with the bulk of the lattice by the massless bonds with the stiffness C_1. Since the displacements are antisymmetric on n, the middle point of each bond between $n=1$ and -1 is fixed; the effective stiffness is thus $2C_1$.

It is convenient to consider equations of motion for particles within an intact lattice, with the forces $q_m(t)$ applied to the masses at the nodes $(m,1)$ along the crack and chosen in such a way that they compensate for the action of vertical bonds connecting the layers of $n=1$ and -1 in the crack region. Namely, behind the crack front we have $q_m(t)=2C_1u_{m,1}(t)$, whereas ahead of the crack $q_m=0$. Then the equations of motion take the form

$$\begin{aligned}
&M_1\ddot{u}_{m,1}(t)=C_1[u_{m+1,1}(t)+u_{m-1,1}(t)+u_{m,2}(t)-5u_{m,1}(t)]+q_m(t)\quad(\text{for } n=1),\\
&M_2\ddot{u}_{m,2}(t)=C_2[u_{m+1,2}(t)+u_{m-1,2}(t)+u_{m,3}(t)-3u_{m,2}(t)]+C_1[u_{m,1}(t)-u_{m,2}(t)]\quad(\text{for } n=2),\\
&M_2\ddot{u}_{m,n}(t)=C_2[u_{m+1,n}(t)+u_{m-1,n}(t)+u_{m,n+1}(t)+u_{m,n-1}(t)-4u_{m,n}(t)]\quad(\text{for } n>2).
\end{aligned}\tag{1}$$

Next we introduce the variable $\eta=m-vt$ associated with the moving coordinate system. The bonds are assumed to brake at $\eta=0$. Thus the crack region is $-\infty<\eta<0$. We now consider a 'steady state' problem where the displacements $u_{m,n}$ depend on η and n only and define

$$u_{m,n}(t)=U_n(\eta),\quad q_m(t)=Q(\eta)=2C_1U_1(\eta)H(-\eta).\tag{2}$$

For the discrete lattice, by saying 'steady state' we mean that

$$u_{m+1,n}(t)=u_{m,n}(t-1/v),\tag{3}$$

for all nodes (m,n).

Applying the Fourier transform with respect to η we deduce

$$M_1(0+\mathrm{i}kv)^2U_1^F(k)=C_1[(2\cos k-5)U_1^F(k)+U_2^F(k)]+Q^F(k)\quad(\text{for } n=1),\tag{4}$$

$$M_2(0+\mathrm{i}kv)^2U_2^F(k)=C_1[U_1^F(k)-U_2^F(k)]+C_2[(2\cos k-3)U_2^F(k)+U_3^F(k)]\quad(\text{for } n=2),\tag{5}$$

$$M_2(0+\mathrm{i}kv)^2U_n^F(k)=C_2[(2\cos k-4)U_n^F(k)+U_{n+1}^F(k)+U_{n-1}^F(k)]\quad(\text{for } n>2),\tag{6}$$

where

$$U_n^F(k)=\int_{-\infty}^{\infty}U_n(\eta)\mathrm{e}^{\mathrm{i}k\eta}\,\mathrm{d}\eta,\quad Q^F(k)=\int_{-\infty}^{\infty}Q(\eta)\mathrm{e}^{\mathrm{i}k\eta}\,\mathrm{d}\eta=2C_1\int_{-\infty}^{0}U_1(\eta)\mathrm{e}^{\mathrm{i}k\eta}\,\mathrm{d}\eta.\tag{7}$$

The solution is sought in the class of functions vanishing as $n\to\infty$.

3. Recurrence relations for a solution of the system (4)–(6)

The dependence of $U_n^F(k)$ on n for $n>2$ is sought in the form

$$U_n^F(k)=\lambda^{n-2}U_2^F(k)\quad\text{with } |\lambda|\le 1.\tag{8}$$

The direct substitution in (6) yields

$$\lambda+\frac{1}{\lambda}=2\Omega(k),\tag{9}$$

where

$$\Omega(k)=2-\cos k+\frac{M_2}{2C_2}(0+\mathrm{i}kv)^2.\tag{10}$$

If $|\Omega(k)|\ge 1$ then λ is real,

$$\lambda=\Omega(k)-\sqrt{\Omega^2(k)-1}\,\mathrm{sign}(\Omega(k)).\tag{11}$$

Otherwise, if $|\Omega|<1$, the quantity λ is complex, and $|\lambda|=1$.

Furthermore, Eqs. (4) and (5) yield

$$U_1^F(k)=\frac{S_2(k,kv)}{S_1(k,kv)}Q^F(k),\quad U_2^F(k)=\frac{C_1}{S_1(k,kv)}Q^F(k),\tag{12}$$

where

$$S_1(k,0+\mathrm{i}k\nu)=[M_1(0+\mathrm{i}k\nu)^2+C_1(5-2\cos k)]S_2(k,0+\mathrm{i}k\nu)-C_1^2,$$
$$S_2(k,0+\mathrm{i}k\nu)=M_2(0+\mathrm{i}k\nu)^2+C_1+C_2(3-2\cos k-\lambda). \tag{13}$$

Note that if $C_1=C_2=C$ then

$$S_2(k,0+\mathrm{i}k\nu)=\frac{C}{\lambda}, \tag{14}$$

and the relation in (8) can be extended to $n=1,2,\ldots$ as follows:

$$U_n^F(k)=\lambda^{n-1}U_1^F(k),\quad |\lambda|\le 1. \tag{15}$$

The function $Q^F(k)$, used in (12), and hence the Fourier transform of the entire solution will be determined in Section 5.

The moving crack is accompanied by waves which may propagate ahead of the crack front and behind the crack front. The first type of waves corresponds to the lattice half-plane with the fixed boundary, whereas the waves behind the crack front are linked to a solution of the problem for the lattice half-plane with the traction free boundary. Correspondingly, the above functions S_1 and S_2 are linked to dispersion properties of waves in a discrete lattice structure occupying a half-plane, which will be the topic of the next section.

4. Dispersion relations for waves in the lattice

We shall use model solutions for a lattice half-plane with the fixed boundary and with the boundary, which is free of tractions. The case of the undamaged lattice half-plane with the fixed boundary corresponds to $Q^F(k)=0$, which is related to a skew-symmetric (in n) deformation of the lattice plane. In the other case of the traction free boundary, we have $Q^F(k)=2C_1U_1^F(k)$.

The dispersion relations, $\omega=\omega(k)$, for the sinusoidal waves along the horizontal layers ($n>1$)

$$f_n\exp[\mathrm{i}(\omega t-km)], \tag{16}$$

with the amplitudes

$$f_1=A_1,\quad f_2=A_2=\frac{C_1A_1}{S_2(k,\mathrm{i}\omega)},\quad f_n=\lambda^{n-2}f_2\ \ (n>2) \tag{17}$$

follow from the above-considered Fourier transforms if the 'inertia term' $0+\mathrm{i}k\nu$ is replaced by $\mathrm{i}\omega$, where ω is the radian frequency. It follows from (14) that $A_2=\lambda A_1$ if $C_1=C_2$.

For the fixed and free boundaries the dispersion relations are written in the form

$$P_1(k,\mathrm{i}\omega)=0\quad \text{where } P_1(k,\mathrm{i}\omega)=S_1(k,\mathrm{i}\omega) \tag{18}$$

and

$$P_2(k,\mathrm{i}\omega)=0\quad \text{where } P_2(k,\mathrm{i}\omega)=S_1(k,\mathrm{i}\omega)-2C_1S_2(k,\mathrm{i}\omega). \tag{19}$$

In these relations, k is the wave number. The phase and group velocities of the wave are $v=\omega/k$ and $\mathrm{d}\omega/\mathrm{d}k$, respectively. The above relations are equivalent to

$$P_1(k,\mathrm{i}\omega)=[-M_1\omega^2+C_1(5-2\cos k)]S_2(k,\mathrm{i}\omega)-C_1^2=0,$$
$$P_2(k,\mathrm{i}\omega)=[-M_1\omega^2+C_1(3-2\cos k)]S_2(k,\mathrm{i}\omega)-C_1^2=0. \tag{20}$$

For the case of $C_1=C_2=C$, according to (14) we deduce

$$P_1(k,\mathrm{i}\omega)=\left(\frac{M_2}{2}-M_1\right)\frac{\omega^2}{C}+3-\cos k+\sqrt{\Omega^2-1}\,\mathrm{sign}(\Omega)=0, \tag{21}$$

$$P_2(k,\mathrm{i}\omega)=\left(\frac{M_2}{2}-M_1\right)\frac{\omega^2}{C}+1-\cos k+\sqrt{\Omega^2-1}\,\mathrm{sign}(\Omega)=0. \tag{22}$$

In particular, if $M_1<M_2/2$, then the acoustical branch in the dispersion diagram is absent, i.e. for any admissible k there are no real roots ω of the dispersion equation within an interval adjacent to the origin. Indeed, otherwise, there must be an interval in k where $0<\omega^2<2C/M_2$, and hence $\Omega=2-\cos k-M_2\omega^2/(2C)>0$. Thus, in this interval, the square root term is

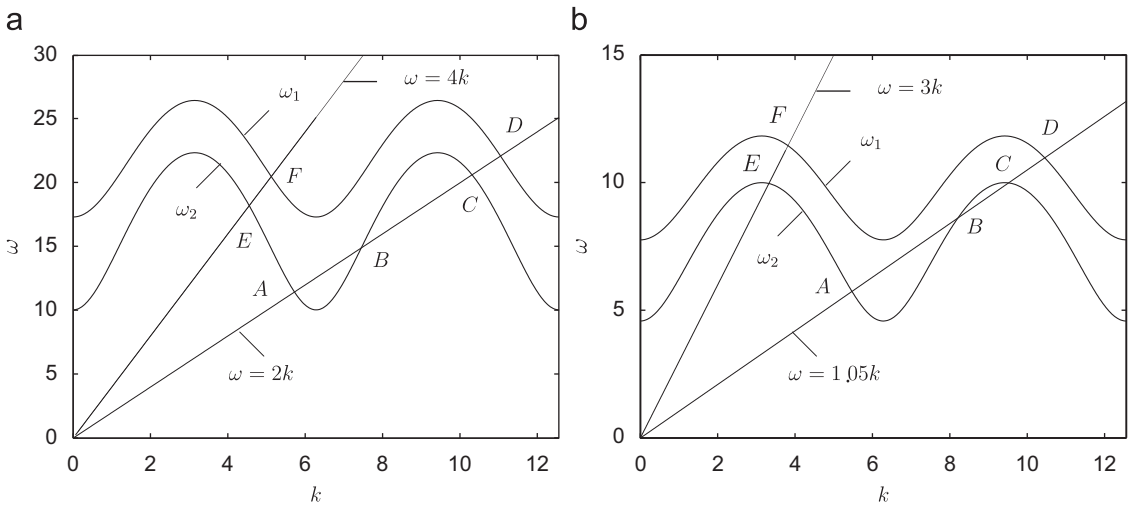

Fig. 2. Dispersion diagrams. (a) $M_1 = 0.01$. The phase speed $v = \omega/k = 2$: thecross-point B corresponds to the feeding knife wave behind the crack front; $v = \omega/k = 4$: the cross-point F corresponds to the feeding knife wave ahead of the crack front. (b) $M = 0.05$. The phase speed $v = \omega/k = 1.05$: the cross-point B corresponds to the feeding knife wave behind the crack front; $v = \omega/k = 3$: the cross-point F corresponds to the feeding knife wave ahead of the crack front.

positive, zero or complex, whereas the other terms in the left-hand side of (21), (22) are positive. Thus neither the first nor the second dispersion relation is satisfied. Eq. (22) is, however, satisfied at the origin: $k = \omega = 0$.

Unless otherwise stated, in the sequel of the paper we consider a lattice of a uniform stiffness, and choose the normalised lattice parameters so that $C_1 = C_2 = 1$ and $M_2 = 1$.

It follows from (21) and (22) that, for the values of M_1, such that $0 < M_1 < \frac{1}{2}$, and for real values of ω, which corresponds to the propagating waves, we have $\Omega < -1$ and $-1 < \lambda < 0$. Thus, in the case of the 'light interface', the waves propagate in the horizontal direction while being exponentially localised in the vicinity of the interface.

The solutions of (21) and (22) are

$$\omega = \omega_{1,2} = \left[-A_{1,2} + \sqrt{A_{1,2}^2 - B_{1,2}}\right]^{1/2}, \tag{23}$$

where

$$A_1 = \frac{5 - 2\cos k - 2M_1(3 - \cos k)}{2M_1(M_1 - 1)}, \quad B_1 = \frac{6 - 2\cos k}{M_1(M_1 - 1)},$$

$$A_2 = \frac{3 - 2\cos k - 2M_1(1 - \cos k)}{2M_1(M_1 - 1)}, \quad B_2 = -\frac{2(1 - \cos k)}{M_1(M_1 - 1)}. \tag{24}$$

The dispersion curves $\omega = \omega_1(k)$ and $\omega = \omega_2(k)$ for $M_1 = 0.01$ and 0.05 are plotted in Figs. 2a and b. The corresponding exponents $\lambda = \lambda_1(k)$ and $\lambda = \lambda_2(k)$, as defined in (11), are shown in Figs. 3a and b. Since $\lambda \ll 1$, according to (15) the waves corresponding to the dispersion relations (23) and shown in Figs. 2a and b are strongly localised around the layer $n = 1$.

The points of intersection of the dispersion curves with the rays $\omega = \text{const}\ k, \omega > 0$, shown in Fig. 2a and b, correspond to the waves propagating with the same phase speed, $v = \omega/k$ for each of the rays. Thus, these waves can be associated with the steady-state regime of the crack propagating with the same speed v. If the group velocity is sufficiently large $v_g = \mathrm{d}\omega_2/\mathrm{d}k > v$ (see point B), then such a wave propagating from behind of the crack front can deliver energy to the crack tip. In the other case of small group velocity $v_g = \mathrm{d}\omega_1/\mathrm{d}k < v$ (see point F), such a wave propagating ahead of the crack front still can deliver energy to the overtaking crack. These waves are referred to as the 'feeding waves' (see Slepyan, 2002).

In Figs. 2a and b, the intersections of the rays $\omega = 2k$ and $\omega = 1.05k$ with the dispersion curves are marked by letters A, B, C and D, whereas the points E and F correspond to the rays $\omega = 4k$ and $\omega = 3k$. We also note that the maximal group velocity in the bulk of the lattice, outside the structural interface, is equal to 1. Thus, the waves corresponding to the intersection points B and F are supersonic with respect to the bulk of the lattice. The strongly localised feeding wave, which supplies the energy to the crack and cuts the bonds, is called here the *knife wave*.

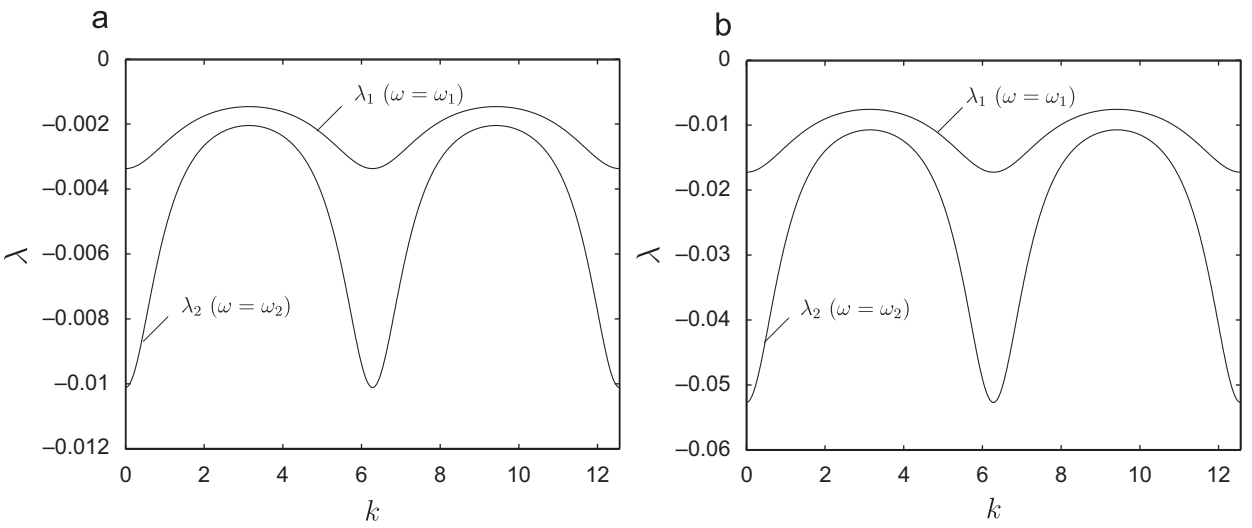

Fig. 3. The exponents λ_1, λ_2. (a) $M_1 = 0.01$, (b) $M_1 = 0.05$.

5. Solution of the crack dynamics problem

We recall that in Section 3 we have derived the Fourier transforms of the solution subject to evaluation of the unknown function Q^F. The present section completes this analysis via reduction of the problem to the functional equation of the Wiener–Hopf type.

The notations $U_{\pm}(k)$ are introduced in such a way that

$$U_1^F(k) = U_-(k) + U_+(k), \tag{25}$$

where

$$U_+(k) = \int_0^{\infty} U_1(\eta)\mathrm{e}^{\mathrm{i}k\eta}\,\mathrm{d}\eta, \quad U_-(k) = \int_{-\infty}^{0} U_1(\eta)\mathrm{e}^{\mathrm{i}k\eta}\,\mathrm{d}\eta. \tag{26}$$

Then Eq. (7) can be rewritten in the form

$$Q^F = 2C_1U_-. \tag{27}$$

From (12) and (27), we have the homogeneous functional equation

$$U_+(k) + L(k)U_-(k) = 0, \tag{28}$$

with

$$L(k) = 1 - \frac{2C_1S_2(k, 0+\mathrm{i}k\nu)}{S_1(k, 0+\mathrm{i}k\nu)} = \frac{P_2(k, 0+\mathrm{i}k\nu)}{P_1(k, 0+\mathrm{i}k\nu)}. \tag{29}$$

Eq. (28) is the functional equation of the Wiener–Hopf type. The kernel functions of this type for a periodic lattice was analysed by Slepyan (2002). It is straightforward to verify that $L(k)$ has a zero index and $L(k)\to 1$ as $k\to\pm\infty$. This enables us to use the Cauchy type integral to factorise this function, that is, to represent it as a product

$$L(k) = L_+(k)L_-(k), \tag{30}$$

with

$$L_{\pm}(k) = \exp\left[\pm\frac{1}{2\pi\mathrm{i}}\int_{-\infty}^{\infty}\frac{\ln L(\xi)}{\xi - k}\,\mathrm{d}\xi\right], \tag{31}$$

where $\pm\Im k > 0$, respectively. Note that for real k

$$|L(-k)| = |L(k)|, \quad \mathrm{Arg}\,L(-k) = -\mathrm{Arg}\,L(k), \tag{32}$$

and the above expression (31) can be rewritten in the form

$$L_{\pm}(k)=\exp\left[\pm\frac{1}{\pi \mathrm{i}}\int_0^{\infty}\frac{k\ln|L(\xi)|+\mathrm{i}\xi\,\mathrm{Arg}\,L(\xi)}{\xi^2-k^2}\,\mathrm{d}\xi\right], \tag{33}$$

with $\pm\Im k>0$, respectively. Also note that Arg $L(k)$ has a finite support. For real k, Eqs. (31) and (32) yield

$$L_{\pm}(-k)=\overline{L_{\pm}(k)}. \tag{34}$$

The factorised form of (28) is

$$\frac{U_+(k)}{L_+(k)}+L_-(k)U_-(k)=0. \tag{35}$$

This equation does not have non-trivial solutions corresponding to bounded displacements at $\eta=0$, which also vanish at infinity. To set up a physical problem, we assume that the energy is supplied to the crack front by a feeding wave coming from $\eta=-\infty$, and correspondingly we introduce the right-hand side as a regularisation of the Dirac delta function, $\delta(k-k_f)$, similar to Slepyan (2002, pp. 400–402). The 'modified' equation (35) is

$$\frac{U_+(k)}{L_+(k)}+L_-(k)U_-(k)=A_f\left[\frac{1}{0+\mathrm{i}(k-k_f)}+\frac{1}{0-\mathrm{i}(k-k_f)}\right], \tag{36}$$

where A_f is an arbitrary complex constant, and the solution has the form

$$U_+(k)=\frac{A_fL_+(k)}{0-\mathrm{i}(k-k_f)},\quad U_-(k)=\frac{A_f}{[(0+\mathrm{i}(k-k_f))]L_-(k)}. \tag{37}$$

According to the physical nature of the problem, the feeding wave arrives from $\eta=-\infty$ and hence $U_-(k)$ has a pole at $k=k_f$, whereas $U_+(k)$ is bounded at that point. This implies that k_f coincides with zero $k=k_B$ of $L_+(k)$, which follows from (29) and is illustrated in Fig. 2.

Note that, in addition to the *delta*-function term $A_f\delta(k-k_f)$, the same function but related to the symmetric zero $k=-k_f$ can be introduced as $B_f\delta(k+k_f)$. Referring to (32) and (33) to get a real solution we take $B_f=\overline{A_f}$. Thus

$$\begin{aligned}U_+(k)&=\frac{A_fL_+(k)}{0-\mathrm{i}(k-k_f)}+\frac{\overline{A_f}L_+(k)}{0-\mathrm{i}(k+k_f)},\\ U_-(k)&=\frac{A_f}{[0+\mathrm{i}(k-k_f)]L_-(k)}+\frac{\overline{A_f}}{[(0+\mathrm{i}(k+k_f))]L_-(k)}.\end{aligned} \tag{38}$$

As it follows from here and (34) for reak k

$$U_{\pm}(-k)=\overline{U_{\pm}(k)} \tag{39}$$

and hence $U(\eta)$ is a real function.

6. Further analysis of feeding and dissipative waves

6.1. Normalisation of $L(k)$

In this section, we consider the cases where the high-speed feeding wave propagates toward the front ($v_g>v$). The background solutions have been given in Section 4. The intersection points of the dispersion curve $\omega_{1,2}(k)$ with the straight line $\omega=kv$, shown in Fig. 2, define zeros of the functions $P_{1,2}$, respectively. The values of k corresponding to the intersection point B in Fig. 2, where the group velocity exceeds the phase speed, are associated with zeros of $L_+(k)$. The other intersection points, where the group velocity is less than the phase speed, and the origin $k=0$ correspond to the singular points of $L_-(k)$. In addition to the positive zeros, there are negative ones placed symmetrically. For the sake of convenience we normalise the functions $L(k)$ and $L_{\pm}(k)$ as follows:

$$\begin{aligned}&L(k)=L^0(k)M_-(k)M_+(k),\quad L^0(k)=L^0_-(k)L^0_+(k),\quad L_-(k)=L^0_-(k)M_-(k),\quad L_+(k)=L^0_+(k)M_+(k),\\ &M_-(k)=\frac{(0+\mathrm{i}k)[0+\mathrm{i}(k-k_A)][0+\mathrm{i}(k+k_A)][0+\mathrm{i}(k-k_C)][0+\mathrm{i}(k+k_C)]}{(1+\mathrm{i}k)[0+\mathrm{i}(k-k_D)][0+\mathrm{i}(k+k_D)](5+\mathrm{i}k)^2},\\ &M_+(k)=\frac{[0-\mathrm{i}(k-k_B)][0-\mathrm{i}(k+k_B)]}{(5-\mathrm{i}k)^2},\end{aligned} \tag{40}$$

where the number '5' can be replaced by any positive number; we take just this value to avoid too large values of the function $\ln|L^0|$.

For the case of $M_1 = 0.01, \nu = 2$ (see Fig. 2a) the wave numbers and the corresponding group velocities (see the points $A,\dots,D$ in Fig. 2a) are $k_A = 5.725200135$ ($v_g = -4.596669685$), $k_B = k_f = 7.451364094$ ($v_g = 6.160892550$), $k_C = 10.31705294$ ($v_g = -3.770776501$), $k_D = 11.05318120$ ($v_g = -4.514179340$). The functions $L^0_{\pm}(k)$ are defined by the relation (31) if $L(\xi)$ is replaced by $L^0(\xi)$. Note that $L^0(k)$ has no zeros and poles (it, however, has singular points associated with zeros of the square root in the expression (11) for λ). Due to (38) and (40), we deduce

$$U_+(k) = \frac{A_f L^0_+(k) M_+(k)}{0 - \mathrm{i}(k - k_f)} + \frac{\overline{A_f} L^0_+(k) M_+(k)}{0 - \mathrm{i}(k + k_f)},$$

$$U_-(k) = \frac{A_f}{[0 + \mathrm{i}(k - k_f)] L^0_-(k) M_-(k)} + \frac{\overline{A_f}}{[(0 + \mathrm{i}(k + k_f))] L^0_-(k) M_-(k)}. \tag{41}$$

Similar normalisation is valid for $M_1 = 0.05, \nu = 1.05$ (see Fig. 2b). In this case $k_A = 5.474451977$ ($v_g = -2.466278976$), $k_B = k_f = 8.214348564$ ($v_g = 2.161418984$), $k_C = 9.524480395$ ($v_g = -0.1986336447$), $k_D = 10.45930645$ ($v_g = -1.563247862$).

6.2. The feeding wave

Let the feeding wave amplitude be $A_0 > 0$. Referring to (38) we take

$$A_f = \tfrac{1}{2} A_0 \Phi, \quad \Phi = L_-(k_f) \mathrm{e}^{-\mathrm{i}\phi}, \tag{42}$$

where ϕ is an 'initial' phase which defines the position of the wave relative to the breaking bond at the crack front, i.e. the point $\eta = 0$. The feeding wave is defined by the values $k = \pm k_f$, and we deduce

$$U_f(\eta) = A_0 \cos(k_f \eta + \phi) H(-\eta). \tag{43}$$

Note that there is no such a wave ahead of the crack. Indeed, in the expression (41) for $U_+(k)$, the explicitly written zeros $k = \pm k_f$ are eliminated by the same zeros of $M_+(k)$ (see (40), $k_B = k_f$).

6.3. The dissipative waves

In both cases, when $M_1 = 0.01,\ \nu = 2$ and $M_1 = 0.05,\ \nu = 1.05$, the dissipative waves are related to the poles of U_- : $k = \pm k_A$ and $k = \pm k_C$. Note that the point $k = k_D$ is a zero of $U_-(k)$ in (38) rather than a pole. Let us denote these waves by $U_A(\eta)$ and $U_C(\eta)$, respectively. We also introduce the quantities

$$L^*_-(k_A) = L^0_-(k_A) \lim_{k \to k_A} \frac{M_-(k)}{0 + \mathrm{i}(k - k_A)}, \quad L^*_-(k_C) = L^0_-(k_C) \lim_{k \to k_C} \frac{M_-(k)}{0 + \mathrm{i}(k - k_C)}. \tag{44}$$

From (40)–(42) we deduce that the dissipative wave amplitudes are

$$W = \frac{2A_0 \sqrt{k_*^2 (\Re\Phi)^2 + k_f^2 (\Im\Phi)^2}}{|k_*^2 - k_f^2| |L^*_-(k_*)|}, \tag{45}$$

where $k_* = k_A$ and $k_* = k_C$ for k_A and k_C-waves, respectively. These waves propagate behind the crack front. There are no waves propagating ahead of the crack.

6.4. Contribution of the pole at $k = 0$

From (40)–(42) it can be found that the pole at $k = 0$ yields a constant displacement as $\eta \to -\infty$:

$$U_0 = -\frac{25 A_0 k_D^2}{k_f k_A^2 k_C^2 L^0_-(0)} \Im\Phi. \tag{46}$$

Note that $L^0_-(0) > 0$. Thus, in addition to the oscillations defined by the feeding and dissipative waves, there is a constant shift of the crack faces relative to each other caused by the oscillating waves (in fact, it tends to a constant as $\eta \to -\infty$). This

phenomenon as a drift of a finite mass or a shift of a semi-infinite waveguide under a harmonic load can be explicitly shown on simple examples (the non-oscillating terms are shown in bold).

Consider a mass, say $M=1$, subject to the oscillatory force $\sin(\omega t+\phi)$. The initial conditions are assumed to be zero. Then the displacement at $t\geq 0$ is

$$u=\frac{\boldsymbol{t}\cos\boldsymbol{\phi}}{\boldsymbol{\omega}}+\frac{\sin\boldsymbol{\phi}}{\boldsymbol{\omega^2}}-\frac{\sin(\omega t+\phi)}{\omega^2}. \tag{47}$$

For an elastic rod, $x>0$, under the same load applied at $x=0$, we find (in terms of the natural units) that the oscillations accompanied by a constant shift propagate as a wave:

$$u(x,t)=\left[\frac{\cos(\boldsymbol{\phi})}{\boldsymbol{\omega}}-\frac{\cos(\omega(t-x)+\phi)}{\omega}\right]H(t-x),\quad t\geq 0. \tag{48}$$

For a semi-infinite chain with the unit masses and stiffness, loaded by this force applied to the first mass, it can be found that, in the subcritical case, $\omega^2<4$, the constant shift is the same as in the previous example. In the supercritical case, $\omega>2$, the high-frequency oscillations do not propagate, and the shift does not exist. However, in this case, a finite amount of the energy goes to the chain. It is the energy of the localised oscillations with the frequency ω and the energy associated with the subcritical frequencies, which appear due to the presence of the initial conditions. All these phenomena appear in the lattice problem, considered in this paper. The constant shift behind the crack (46) is associated with a region of the subcritical frequencies, and the energy redistributed between the waves is produced by the high-frequency oscillations, as described in Section 10.

7. Alternating strain: $\boldsymbol{u_{m,n}(t)=U_n(\eta)(-1)^m}$

For mode III deformation and fracture caused by a sinusoidal wave, a different 'steady-state' regime of the crack growth in the considered square lattice can be envisaged. It can be assumed that the sequence of the bond ruptures takes place in equal time-intervals, as in the above-considered regime, but with alternating signs of the critical strain. Thus we now assume that the displacements can be represented in the form

$$u_{m,n}(t)=U_n(\eta)(-1)^m,\quad \eta=m-vt. \tag{49}$$

With respect to a sinusoidal wave propagating in the m-direction this means that

$$u_{m,n}(t)=A_n e^{-i[\omega(k)t-km]}(-1)^m=A_n e^{-i[\omega(k)t-(k-\pi)m]}. \tag{50}$$

The latter expression is suitable for the continuum representation of the wave where m can be considered as a continuous variable; on the other hand, for the discrete system, only the integer values of the coordinate are important. Let $U_n^F(k)$ denote the Fourier transform of $u_{m,n}$ for an even $m=0,\pm 2,\ldots$

$$U_n^F(k)=\int_{-\infty}^{\infty}U_n(\eta)e^{ik\eta}\,d\eta. \tag{51}$$

Then for any odd m

$$[u_{m,n}(t)]^F=-U_n^F(k),\quad m=\pm 1,\pm 3,\ldots\ . \tag{52}$$

We now rewrite the equations for the alternating-strain regime. Using Eqs. (1) and (49) we obtain (compare with (4)–(6))

$$M_1(0+ik\nu)^2U_1^F(k)=C_1[-(2\cos k+5)U_1^F(k)+U_2^F(k)]+Q^F(k)\quad(\text{for } n=1), \tag{53}$$

$$M_2(0+ik\nu)^2U_2^F(k)=C_1[U_1^F(k)-U_2^F(k)]+C_2[-(2\cos k+3)U_2^F(k)+U_3^F(k)]\quad(\text{for } n=2), \tag{54}$$

$$M_2(0+ik\nu)^2U_n^F(k)=C_2[-(2\cos k+4)U_n^F(k)+U_{n+1}^F(k)+U_{n-1}^F(k)]\quad(\text{for } n>2). \tag{55}$$

Next, among the relations of Section 3, only (10) and (13) have now been changed to become

$$\Omega(k)=2+\cos k+\frac{M_2}{2C_2}(0+ik\nu)^2, \tag{56}$$

and

$$S_1(k,0+\mathrm{i}kv) = [M_1(0+\mathrm{i}kv)^2 + C_1(5+2\cos k)]S_2(k,kv),$$

$$S_2(k,0+\mathrm{i}kv) = M_2(0+\mathrm{i}kv)^2 + C_1 + C_2(3+2\cos k - \lambda), \tag{57}$$

whereas the remaining relations are still as they are. Accordingly, in Section 4, the relations (20)–(22) become

$$P_1(k,\mathrm{i}\omega) = [-M_1\omega^2 + C_1(5+2\cos k)]S_2(k,\mathrm{i}\omega) - C_1^2 = 0,$$

$$P_2(k,\mathrm{i}\omega) = [-M_1\omega^2 + C_1(3+2\cos k)]S_2(k,\mathrm{i}\omega) - C_1^2 = 0, \tag{58}$$

and in the case of $C_1 = C_2 = C$ (see (11) and (14)) we have

$$P_1(k,\mathrm{i}\omega) = \left(\frac{M_2}{2} - M_1\right)\frac{\omega^2}{C} + 3 + \cos k + \sqrt{\Omega^2 - 1}\,\mathrm{sign}(\Omega) = 0, \tag{59}$$

$$P_2(k,\mathrm{i}\omega) = \left(\frac{M_2}{2} - M_1\right)\frac{\omega^2}{C} + 1 + \cos k + \sqrt{\Omega^2 - 1}\,\mathrm{sign}(\Omega) = 0. \tag{60}$$

The statement concerning the absence of the acoustical branch is still valid in this case. Now the zero at the origin does not exist, and hence there is no constant shift term for the displacement at $\eta \to -\infty$.

The quantities in the relation (23) become

$$A_1 = \frac{5+2\cos k - 2M_1(3+\cos k)}{2M_1(M_1-1)}, \quad B_1 = \frac{6+2\cos k}{M_1(M_1-1)},$$

$$A_2 = \frac{3+2\cos k - 2M_1(1+\cos k)}{2M_1(M_1-1)}, \quad B_2 = -\frac{2(1+\cos k)}{M_1(M_1-1)}. \tag{61}$$

The dispersion curves are presented in Fig. 4 for $M_1 = 0.1$, $v = 1.15$, and the related exponents λ are shown in Fig. 5. The corresponding wave numbers (as the cross-points $\omega_{1,2}$ on the ray $\omega = 1.25k$) are: $k_A = 2.944022994$ ($v_g = -0.5252941955$), $k_B = k_f = 4.575226946$ ($v_g = 1.853576372$), $k_C = 6.152173545$ ($v_g = 0.1837938996$), $k_D = 7.013954860$ ($v_g = -0.8253775985$).

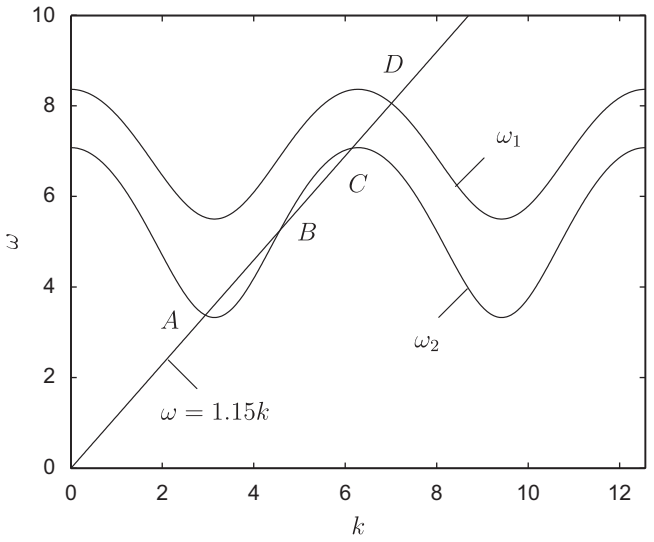

Fig. 4. Dispersion diagram for the alternating-strain regime, $M_1 = 0.1$. The cross-points correspond to the phase speed $v = \omega/k = 1.15$.

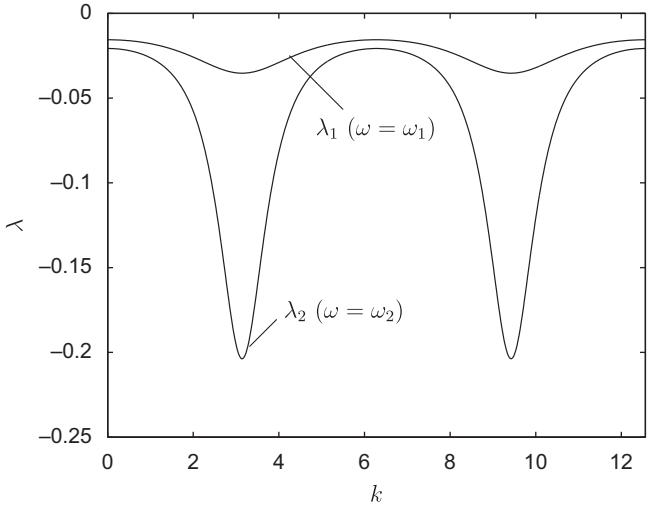

Fig. 5. The exponents λ_1, λ_2 for the case $M_1 = 0.1$.

8. High-contrast interface approximation, and numerical simulation

8.1. The lattice strip

In the above-considered examples, $|\lambda| \ll 1$. Hence the oscillation amplitudes outside the interface are very small relatively those in the line $n = 1$. Since the energy is a quadratic function of the amplitudes, it follows that almost all the energy of the waves is contained in the interface. Besides, only an infinitesimal amount of the energy is radiated from the interface to the bulk of the lattice.

This suggests that a good approximation of the lattice dynamics, incorporating the wave amplitudes and the energy fluxes, can be achieved through an analysis of a one-dimensional model. The latter can be constructed by assuming that the masses outside the interface, i.e. on the lines $n > 1$, are fixed, and the waveguide itself consists of the interface particles only. Here we keep this approximation and assume that the masses on the line $n = 2$ are stationary.

We consider the chain $m = 0, 1, \ldots, m_{end} = 200$ with the initial crack at $m = 0, 1, \ldots, m_*(0) = 51$. Under zero initial conditions the system of ordinary differential equations is

$$\begin{aligned} &u_0 = A\sin\omega_f^0 t H(t), \quad u_{m_{end}} = 0, \\ &\ddot{u}_m = -3u_m + u_{m-1} + u_{m+1} \quad (m < m_*(t)), \\ &\ddot{u}_m = -5u_m + u_{m-1} + u_{m+1} \quad (m \geq m_*(t)), \end{aligned} \tag{62}$$

where $m_*(t)$ is the crack front. At the moment when u_m first reaches the critical value, the corresponding bond (below the mass) breaks and m_* receives a unit increment.

For such a lattice strip

$$\begin{aligned} &\omega = \omega_1^0(k) = \sqrt{5 \mp 2\cos k} \quad \text{for the intact chain,} \\ &\omega = \omega_2^0(k) = \sqrt{3 \mp 2\cos k} \quad \text{for the crack region boundary condition,} \end{aligned} \tag{63}$$

where the signs $\mp$ correspond to the steady-state and alternating-strain regimes, respectively; the mass of each particle is taken to be unity. The dispersion diagrams $\omega_2^0(k)$ are plotted in Fig. 6. With the reference to the above-considered cases we now have to take, in the one-dimensional model, the frequency $\omega_f^0 = \omega_f\sqrt{M_1}$, and we may expect to obtain the crack speed as theoretically predicted: $V = v\sqrt{M_1}$. For the numerical simulations, we take $V = V_{steady} = 0.2$ for the steady-state regime, that relates to the case $M_1 = 0.01$, $v = 2$ considered in Section 6. From the dispersion relation $\omega_2^0(k)$ in (63) it follows that $k_f = 7.455033153$, $\omega_2^0 = 1.491006630$, $V_g = 0.6180186908$. We take the same frequency for the alternating-strain case; using the first dispersion relation from (63) we thus have $V = V_{alternate} = 0.3456652828$, $k_f = 4.313440499$, $\omega_2^0 = 1.491006630$, $V_g = 0.6180186908$.

8.2. Critical amplitude of the feeding wave

First we find the feeding wave amplitude which is required for an initial crack to grow. In the numerical simulations, we assume that only the crack-line bonds can be broken. Consider an established regime where the complex wave

$$u_I = A_0 e^{i(\omega t - km)} \tag{64}$$

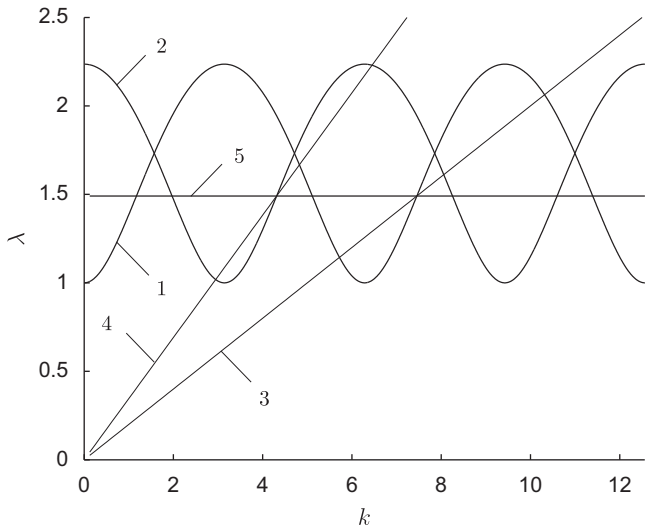

Fig. 6. The lattice strip dispersion diagram, $\omega_2^0(k)$, for the steady-state regime (1) and for the alternating-strain regime (2). The corresponding phase speeds are defined by the rays 3 and 4. Horizontal line 5 corresponds to the frequency $\omega^0 = 1.491006630$.

propagating toward the stationary crack front, $m = 0$, is accompanied by the reflected and transmitted waves as

$$u_R = A_R e^{i(\omega t + km)} \ (m \le 0), \quad u_T = A_T \lambda^m e^{i\omega t} \ (m \ge 0, \lambda < 1), \tag{65}$$

where it is assumed that $1 < \omega^2 < 3$ (in this region, no propagating wave exists at $m > 0$). From the last equation in (62) it follows that

$$\lambda = \frac{5-\omega^2}{2} - \sqrt{\left(\frac{5-\omega^2}{2}\right)^2 - 1}. \tag{66}$$

From the displacement continuity and dynamic equilibrium conditions at $m = 0$ we find

$$A_T = A_0 + A_R = A_0 \frac{2i \sin k}{1/\lambda - \exp(-ik)} \quad \left(\cos k = \frac{3-\omega^2}{2}\right). \tag{67}$$

The critical value of the amplitude at $m = 0$ is equal to the displacement breaking the bond, that is

$$A_0 \left| \frac{2i \sin k}{1/\lambda - \exp(-ik)} \right| = u_c \implies \mathscr{A} = \frac{A_0}{u_c} = \mathscr{A}^* = \left| \frac{1/\lambda - \exp(-ik)}{2 \sin k} \right|. \tag{68}$$

Thus, for the crack to grow the feeding wave amplitude must be greater than this value. The plot of this limiting dependence is presented in Fig. 7.

8.3. Crack speeds

Two formulations related to the high-contrast interface are analysed numerically: the steady-state formulation with the fracture criterion $u_m = u_c > 0$, and the alternate-strain formulation with the fracture criterion $|u_m| = u_c > 0$. Recall that for both cases we take the same frequency $\omega = 1.491006630$; the other parameters of the feeding waves are listed in Section 8.1. The numerical simulations show that, in certain regions of $\mathscr{A}$, these regimes are established with the corresponding (theoretically predicted) crack speeds.

Figs. 8a and b give the numerically obtained crack speed, under the *steady-state criterion*, as a function of $\mathscr{A}$. If $\mathscr{A} < \mathscr{A}^* = 1.176770982$, the crack growth, even if initiated, stops. As $\mathscr{A} > \mathscr{A}^*$ the crack propagates, and the crack speed is independent of the amplitude within the interval $\mathscr{A} \in (\mathscr{A}^*, 2.18]$; this crack speed is equal to the theoretically predicted speed $V_{steady} = 0.2$. On the other hand, further increase in the amplitude results in the increase of the average crack speed, $\langle V \rangle$ which approaches the value of the feeding wave group velocity $V_g = 0.6180186908$ as $\mathscr{A} \to \infty$.

It is worth mentioning that the crack itself is not steady in this case. Figs. 8a and b show the jump-like increase of the crack speed for certain values of the increasing amplitude of the feeding wave. It is also remarked that there exists an interval of amplitudes where the crack speed is approximately constant, and it is equal to the alternating-strain regime.

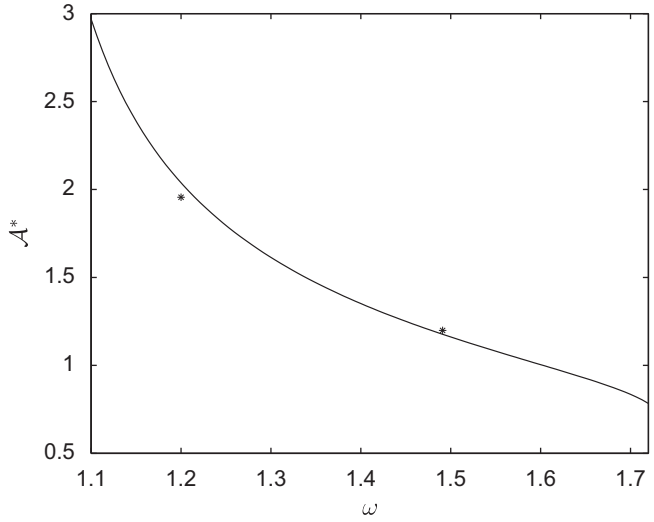

Fig. 7. The lower bound of the ratio of the feeding wave amplitude to the critical elongation of the bond on the crack path, $\mathscr{A} = A_0/u_* = \mathscr{A}^*$ as a function of the frequency. The asterisks correspond to the numerically obtained values.

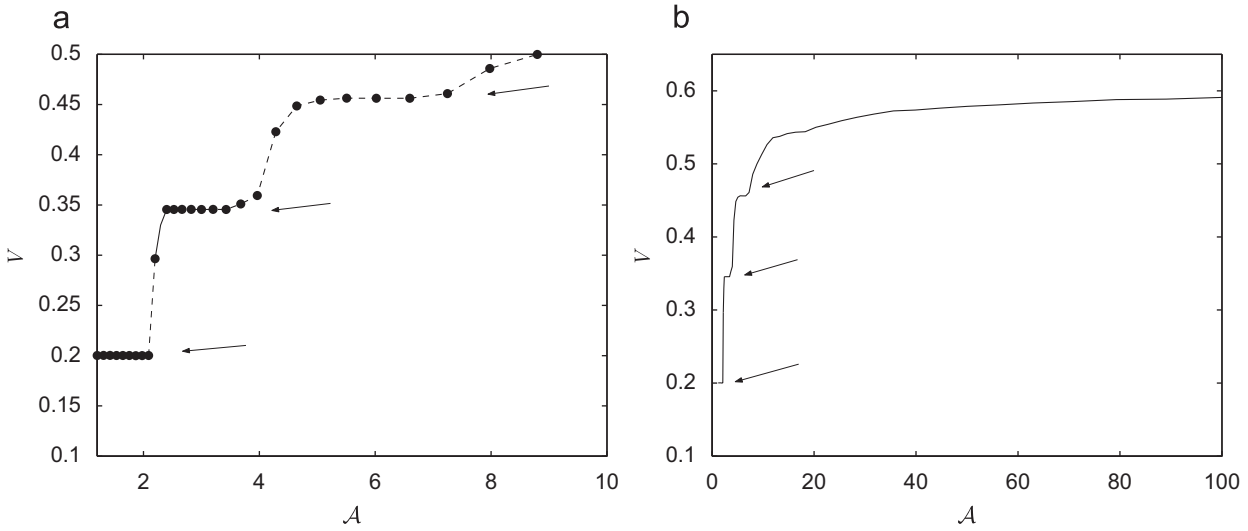

Fig. 8. The crack speed as a function of the amplitude of the feeding wave. The calculations were conducted under the steady-state regime related fracture criterion, $u_m = u_c > 0$. (a) $\mathscr{A}^* < \mathscr{A} < 10$, (b) $\mathscr{A}^* < \mathscr{A} < 100$.

Fig. 8b also shows that for sufficiently large values of the amplitude $\mathscr{A}$ the averaged crack speed approaches the group velocity of the feeding wave.

In Fig. 9 we show the position of the crack front as a function of time for different amplitudes of the feeding wave. In particular, for the two chosen values, $\mathscr{A} = 1.2$ and 2.0, the speeds of the crack are the same, and the time-interval between the breakage of the neighbouring bonds is constant, equal to $1/V$ that corresponds to the steady-state regime. At the higher values of the amplitude, the averaged speed is established as $\mathscr{A}$-dependent constant, whereas the local crack speed is non-uniform; it oscillates between the steady-state value, $V = 0.2$, and a higher value, $V \approx 0.8$. As can be seen in Fig. 9, large clusters within the lattice correspond to the higher speed, whereas the lower, theoretically predicted ($V = 0.2$) corresponds to the local speed between the clusters.

This non-uniformity in the local crack speed is shown in more detail in Fig. 10. This mode of fracture can be called the *oscillating crack-speed regime*. As shown in Fig. 10, at a very large amplitude multiple local speeds arise; however, even in such a locally disordered crack growth, the averaged (macrolevel) crack speed is established; it is a function of the amplitude only.

Under the *alternating-strain criterion*, the crack speed dependence is presented in Figs. 11a and b. First, $\mathscr{A}^* < \mathscr{A} < 1.35$, the speed coincides with that for the steady-state criterion. Then as $\mathscr{A}$ further increases, the speed also increases to form

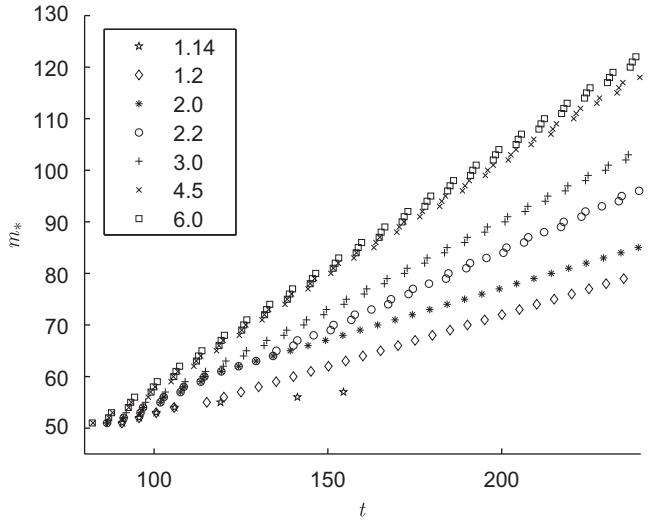

Fig. 9. Positions of the crack front, m_*, versus time, t. The calculations were conducted under the steady-state related fracture criterion, $u_m = u_c > 0$. The values of the amplitude, $\mathscr{A}$, are shown in the insert. The steady-state regime is established with $V = 0.2$ for $\mathscr{A} = 1.2$ and 2.0. The oscillating crack speed regime is established with the increased averaged speeds for $\mathscr{A} = 2.2, \ldots, 6.0$.

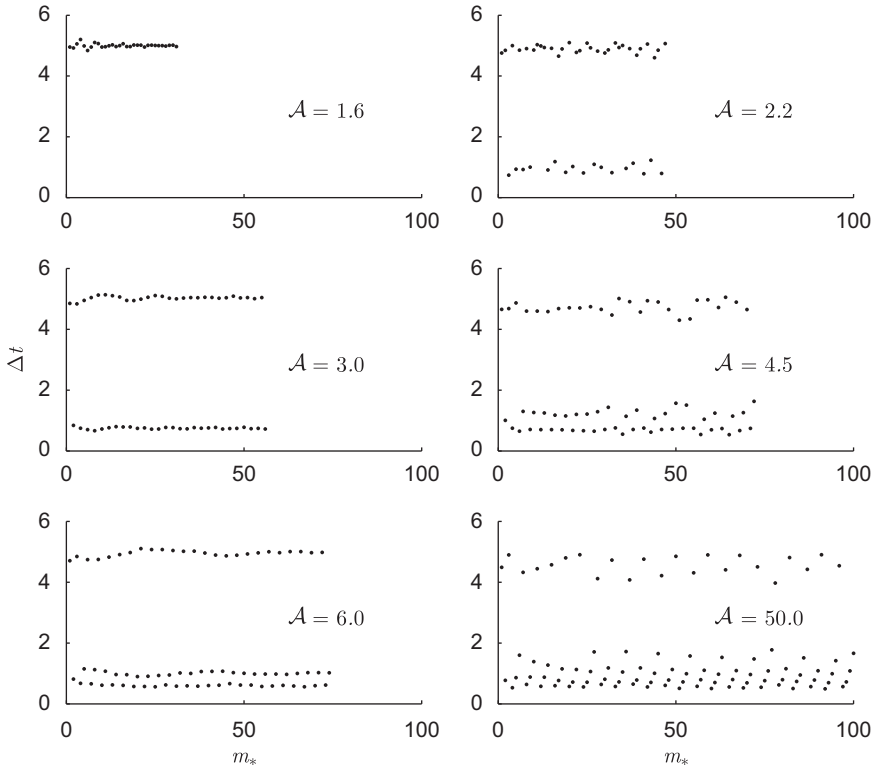

Fig. 10. The intervals between the breakage of the neighbouring bonds, Δt, versus the sequence of the breakages of the bonds, m_*, in the criterion related to the steady-state regime, $u_m = u_c$.

the oscillating crack-speed regime, which corresponds $\mathscr{A} \in (1.35, 1.85)$. In the further increase of the amplitude, the alternating-strain regime is established where the crack speed is equal to the predicted value, $V = V_{alternate} = 0.3456652828$, which corresponds to $\mathscr{A} \in (1.85, 2.51)$. As the amplitude becomes greater the oscillating crack-speed regime occurs again. The results of the numerical simulations under this criterion are illustrated in Figs. 11a and b, 12 and 13, which are of the same nature as Figs. 8a and b, 9 and 10, respectively.

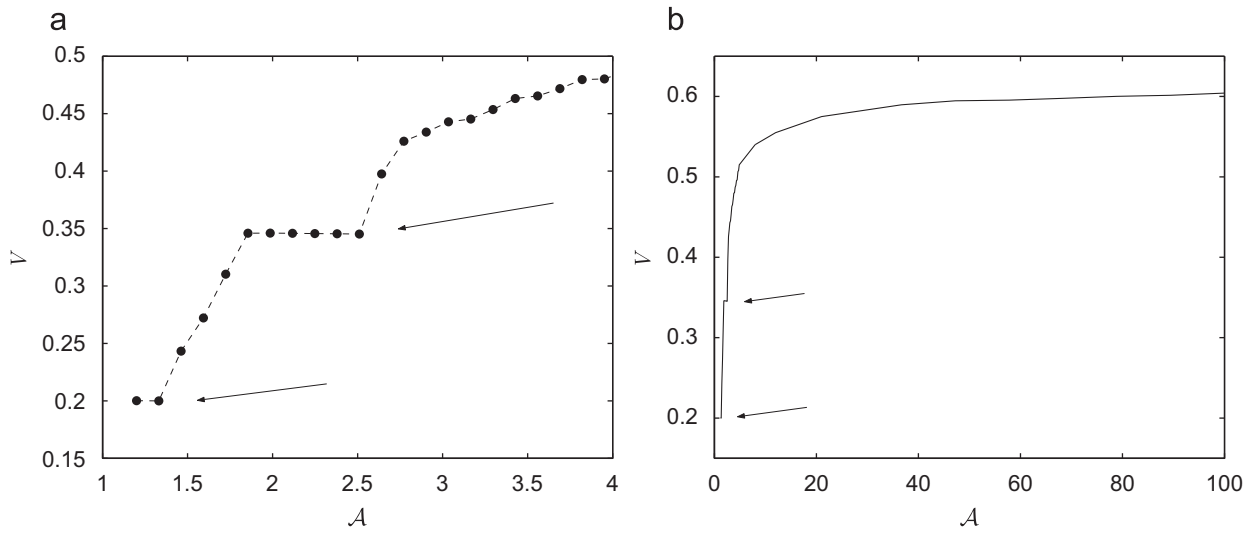

Fig. 11. The crack speed, V, as a function of the amplitude of the feeding wave, $\mathcal{A}$. The calculations were conducted under the alternating-strain fracture criterion, $|u_m| = u_c > 0$. (a) $\mathcal{A}^* < \mathcal{A} < 4$, (b) $\mathcal{A}^* < \mathcal{A} < 100$.

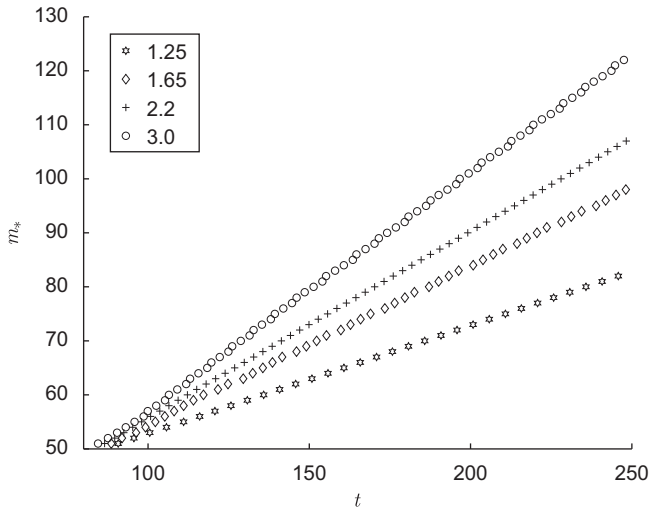

Fig. 12. Positions of the crack front, m, at its break moment versus time, t. The calculations were conducted under the alternating-strain fracture criterion, $|u_m| = u_c > 0$. The values of the amplitude, $\mathcal{A}$, are listed in the insert. The steady-state regime occurs with $V = 0.2$ for $\mathcal{A} = 1.25$ and the alternating-strain regime is established with $V = V_{alternate} = 0.3456652828$ for $\mathcal{A} = 2.2$. The oscillating crack speed regime is established for $\mathcal{A} = 1.65$ and 3.0.

9. Other types of structural interfaces

In addition to the configurations incorporating high-contrast interface described above, we draw attention of the reader to the fact that localised knife waves can be supported by interfaces of other types. Some of such examples are outlined here.

9.1. The low-contrast structural interface

In the above analysis, the feeding wave was delivered along the crack surface, from minus infinity to the crack front. Thus, the group velocity of the wave must exceed the crack speed, and the supersonic crack can exist only in the case of a high-contrast structural interface.

As shown in Slepyan (1981, 2002), the feeding wave can be characterised by the delta-function term in the right-hand side of the homogeneous equation (35). The 'support' of such right-hand side coincides with a zero of $L_+(k)$—when the feeding wave is behind the crack front, and with a pole of $L_-(k)$—when the feeding wave is ahead of the crack. As shown in

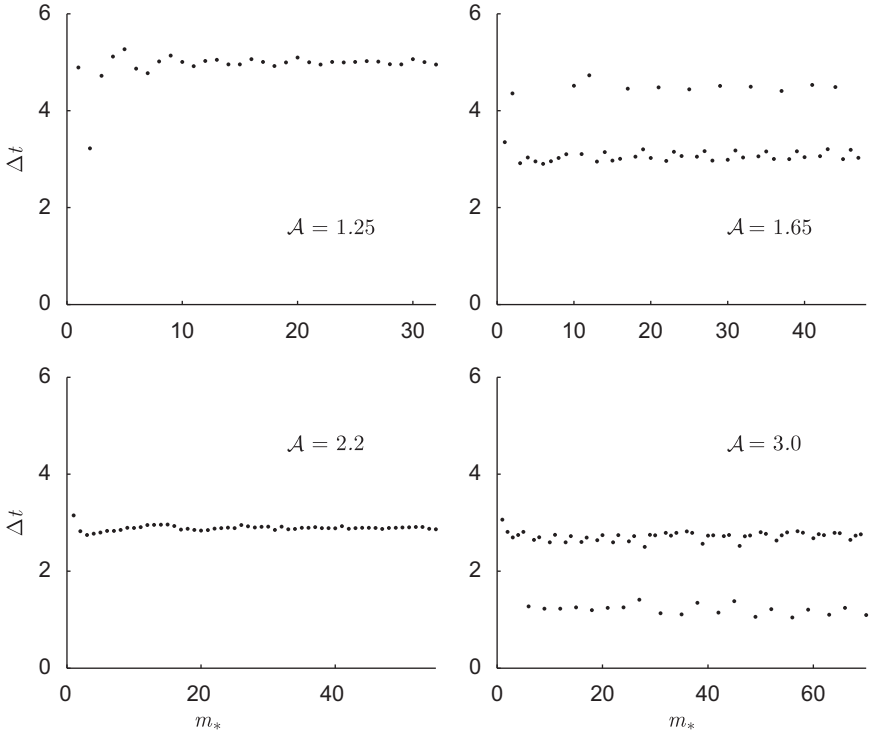

Fig. 13. The intervals between the breakage of the neighbouring bonds versus the sequence of the breakages of the bonds, in the case of the alternating crack-speed criterion, $|u_m| = u_c$.

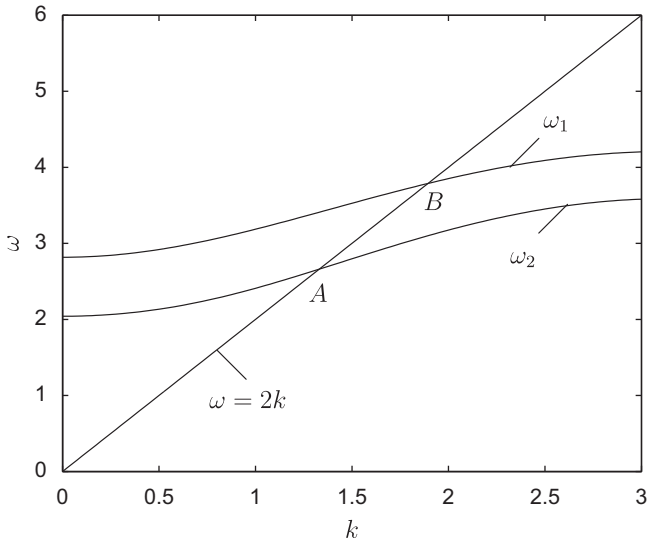

Fig. 14. Dispersion diagram for the low-contrast interface, $M_1 = 0.4$. The intersection points A and B correspond to the phase speed $v = 2$.

Fig. 2, the latter type of the feeding wave can exist and corresponds to the wave number k_D. In this case the dissipative wave numbers are k_A and k_C.

Thus, the feeding wave may also be placed in front of the crack. For such a configuration, the group velocity of the wave must be less than the crack speed, and we show in the text below that the fracture supported by such a feeding wave can also exist for low-contrast structural interfaces.

The low-contrast case for the steady-state regime, $M_1 = 0.4,\ v = 2$, is illustrated in Figs. 14 (the dispersion diagram) and 15 (the corresponding exponents characterising the rate of localisation). Now the feeding wave is placed ahead the crack front; k_B is its wave number corresponding to the intersection point B, and the dissipative wave placed behind the crack

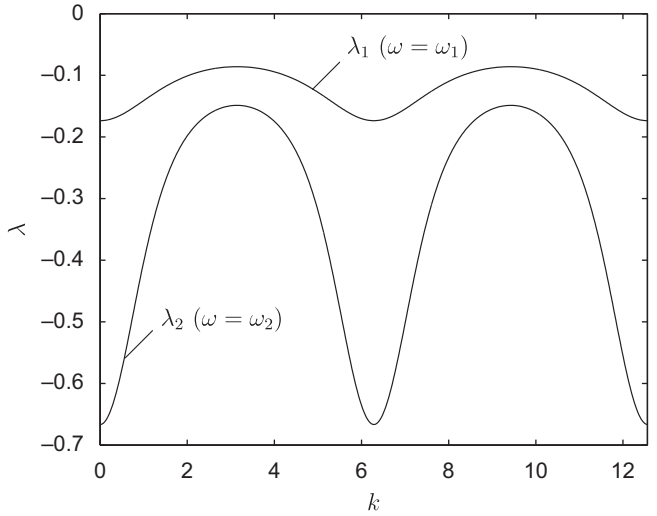

Fig. 15. The exponents λ_1, λ_2 for the case $M_1 = 0.4$.

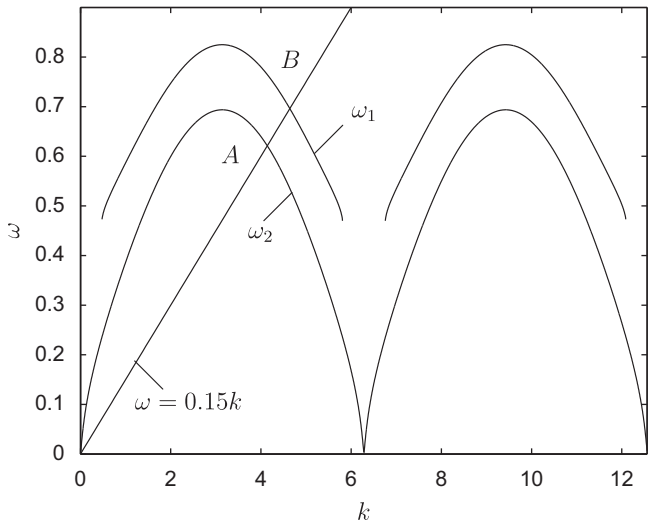

Fig. 16. Dispersion diagram for the heavy interface, $M_1 = 10$. The cross-points correspond to the phase speed $v = 0.15$.

front; k_A is its wave number corresponding to the point A. We represent the function $L(k)$ in the way similar to (40)

$$
\begin{aligned}
&L(k) = L^0(k)M_-(k), \quad L^0(k) = L^0_-(k)L^0_+(k),\\
&L_-(k) = L^0_-(k)M_-(k), \quad L_+(k) = L^0_+(k),\\
&M_-(k) = \frac{(0+\mathrm{i}k)[0+\mathrm{i}(k-k_A)][0+\mathrm{i}(k+k_A)]}{(1+\mathrm{i}k)[0+\mathrm{i}(k-k_B)][0+\mathrm{i}(k+k_B)]},
\end{aligned}
\tag{69}
$$

where $k_A = 1.330321963$ ($v_g = 0.7989444170$), $k_B = k_f = 1.893929503$ ($v_g = 0.6158398400$). The expressions (41) for $U_\pm(k)$ are still valid, and $M_+(k) = 1$. Consequently, the feeding and dissipative waves are defined by the expressions (43) and (45) with the above values of k_A and k_B.

9.2. Localisation within a heavy structural interface ($M_1 > 1$)

In this section we show that the localised knife wave can exist in the case of a heavy interface, when $M_1 > M_2 = 1$. We consider an example where $M_1 = 10$, $v = 0.15$, and give the dispersion diagram and the graphs of the localisation exponents in Figs. 16 and 17, respectively. Here k_B is the wave number for the feeding wave placed ahead of the crack ($k_B = 4.640727636$, $v_g = -0.1556902544$), and k_A corresponds to the dissipative wave ($k_A = 4.140924115$, $v_g = -0.1417943765$). The feeding and dissipative waves are defined by the expressions (43) and (45).

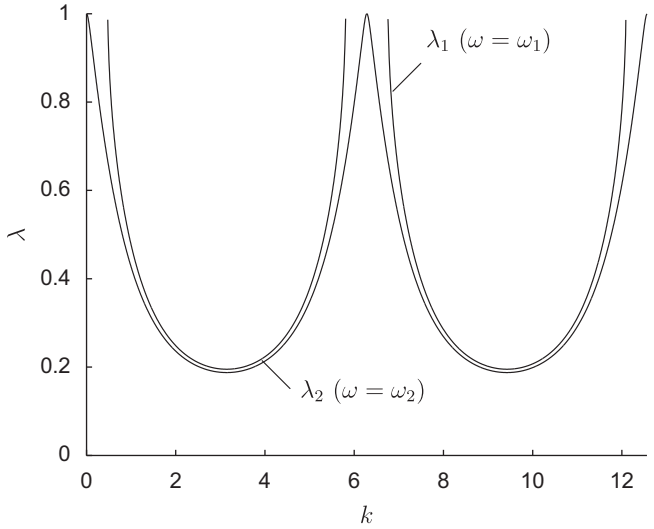

Fig. 17. The exponents λ_1, λ_2 for the case $M_1 = 10$.

10. Energy relations

In this section we address the fundamental relations of the energy balance. The emphasis is on the dissipation associated with the localised waves, which carry the energy away from the 'crack tip'. We also determine the energy percolating to the bulk of the lattice. We make a comparative analysis of the lattice strip problem and the problem of the structural interface separating two lattice half-planes. The effects of localisation are clearly visible in the latter results.

10.1. General dependencies

For a localised sinusoidal wave (17) the energy flux, N, is defined as the product of the force acting on a particle from the left, and its velocity. From (17) it can be found that the energy flux in the wave propagating in the crack area is

$$N = \frac{1}{2}|A_1|^2 k v \sin k \left[1 + \frac{C_1}{S_2^2(k, \mathrm{i}\omega)[1-\lambda^2(k)]}\right], \tag{70}$$

where A_1 is the complex wave amplitude, k is the wave number, $\lambda(k)$ is the corresponding exponent and v is the phase velocity. It follows from (14) that if $C_1 = C_2$ then the above relation is reduced to

$$N = \frac{1}{2}|A_1|^2 \frac{k v \sin k}{1-\lambda^2(k)}. \tag{71}$$

For a wave with parameters k, λ and $v_g = \mathrm{d}\omega/\mathrm{d}k$, the energy release rate is given by

$$G = \frac{N}{v v_g}|v_g - v|. \tag{72}$$

In particular, for the feeding wave $G = G_f$ is the energy carried to the crack front, whereas for a dissipative wave this is the energy radiated from the crack front. Note that the group velocity can be positive, zero or negative, but, in the considered structures, the ratio $(\sin k)/v_g$ is always positive and bounded, which guarantees that the quantity (72) is also positive and bounded.

10.2. The energy radiated from the interface

We consider the energy flux from the node (m, n) to the node $(m, n+1)$. We note that the answer will not depend on m. The total energy transfer is

$$G_r = G_{n\to n+1} = \int_{-\infty}^{\infty} [u_{m,n}(t) - u_{m,n+1}(t)]\dot{u}_{m,n+1}(t)\,\mathrm{d}t. \tag{73}$$

Using the Parseval identity and taking into account that

$$U^F_{n+1}(k) = U^F_n(k)\lambda(k) = U^F_2(k)\lambda^{n-1}(k) \quad (n \geq 2) \tag{74}$$

we can express (73) in the form

$$\begin{aligned} G_r &= -\int_{-\infty}^{\infty} [U_n(\eta) - U_{n+1}(\eta)] \frac{\mathrm{d}U_{n+1}(\eta)}{\mathrm{d}\eta}\, \mathrm{d}\eta = -\frac{1}{2\pi}\int_{-\infty}^{\infty} [U^F_n(k) - U^F_{n+1}(k)]\overline{(-\mathrm{i}k)U^F_{n+1}(k)}\, \mathrm{d}k \\ &= -\frac{1}{2\pi}\int_{-\infty}^{\infty} |U^F_2(k)|^2 [1 - \lambda(k)]|\lambda|^{n-2}\overline{(-\mathrm{i}k)\lambda(k)}\, \mathrm{d}k, \end{aligned} \tag{75}$$

where in accordance with (4)

$$U^F_2(k) = \left(5 - 2\cos k - \frac{M_1}{C_1}k^2\nu^2\right)U_+(k) + \left(3 - 2\cos k - \frac{M_1}{C_1}k^2\nu^2\right)U_-(k). \tag{76}$$

Only the imaginary part of $\lambda(k)$ gives a contribution to the integral (75). In the corresponding domain, $|\lambda(k)| = 1$ and the integral becomes

$$G_r = \frac{1}{\pi}\int_{\mathscr{K}} |U^F_2(k)|^2 \sqrt{1 - \Omega^2}\, k\, \mathrm{d}k, \tag{77}$$

where the domain $\mathscr{K}$ is a subset of the positive semi-axis $k > 0$, where $\Omega^2 < 1$. The radiated energy as a function of ϕ is plotted in Fig. 18, which shows the lower energy radiation for the higher contrast of the interface.

10.3. The energy of the bond

The strain energy of the broken bond is

$$G_0 = U^2(0), \tag{78}$$

where the total displacement at the moment of the bond breakage can be obtained from (38) and (42) as the limit

$$U(0) = \lim_{s\to\infty} sU_+(\mathrm{i}s) = \lim_{s\to\infty} sU_-(-\mathrm{i}s) = A_0 \Re\Phi. \tag{79}$$

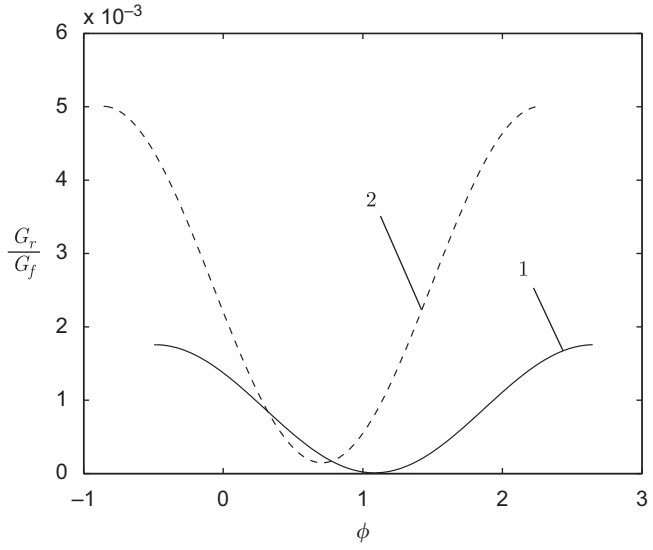

Fig. 18. The ratio of the energy radiated from the interface to the feeding wave energy: $M_1 = 0.01,\ \nu = 2$ (1) and $M_1 = 0.05,\ \nu = 1.05$ (2).

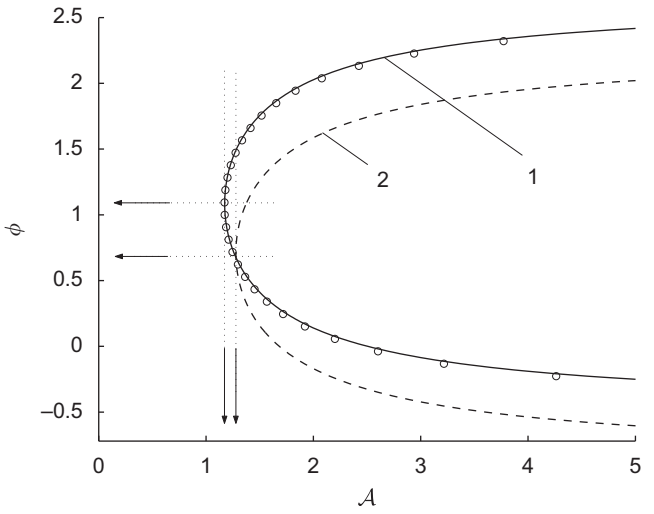

Fig. 19. The normalised amplitude of the feeding wave, $\mathscr{A}$, versus the 'initial phase' ϕ. Curves (1) and (2) correspond to the two-dimensional lattice, where $M_1 = 0.01,\ \nu = 2$; $\mathscr{A} = \mathscr{A}_{\min} = 1.174$ at $\phi = 1.0849$ (1) and $M_1 = 0.05,\ \nu = 1.05$; $\mathscr{A} = \mathscr{A}_{\min} = 1.278$ at $\phi = 0.7076$ (2). The circles correspond to the lattice strip.

Now, using the deformational fracture criterion, we deduce

$$\Re\Phi \equiv \Re[L_-(k_f)\mathrm{e}^{-\mathrm{i}\phi}] = \frac{1}{\mathscr{A}} = \frac{u_c}{A_0}, \tag{80}$$

where u_c is the critical elongation of the elastic bond.

Given the feeding wave amplitude, A_0, and the critical elongation u_c, this relation can be used to determine the initial phase ϕ. On the contrary, we can fix ϕ and determine the relations between the amplitudes of the feeding and dissipative waves and the critical elongation of the bond. The dependence of the normalised amplitude, $\mathscr{A}$, on the phase ϕ is plotted in Fig. 19. In particular, these computations show an excellent agreement between the case of the high-contrast interface ($M_1 = 0.01$) and the lattice strip model.

10.3.1. The energy relation for the lattice strip

Consider the steady-state regime. The kernel $L(k)$ can be represented as in (40) (now $L(0) \neq 0$):

$$L(k) = \frac{3 + (0 + \mathrm{i}kV)^2 - 2\cos k}{5 + (0 + \mathrm{i}kV)^2 - 2\cos k} = L^0(k)M_-(k)M_+(k), \quad L^0(k) = L^0_-(k)L^0_+(k),$$

$$L_-(k) = L^0_-(k)M_-(k), \quad L_+(k) = L^0_+(k)M_+(k),$$

$$M_-(k) = \frac{[0 + \mathrm{i}(k - k_A)][0 + \mathrm{i}(k + k_A)][0 + \mathrm{i}(k - k_C)][0 + \mathrm{i}(k + k_C)]}{[0 + \mathrm{i}(k - k_D)][0 + \mathrm{i}(k + k_D)](5 + \mathrm{i}k)^2},$$

$$M_+(k) = \frac{[0 - \mathrm{i}(k - k_B)][0 - \mathrm{i}(k + k_B)]}{(5 - \mathrm{i}k)^2}, \tag{81}$$

where for $V = 0.2$ the wave numbers are $k_A = 5.720095950$, $k_B = k_f = 7.455033153$, $k_C = 10.31605445$, $k_D = 11.05246522$. Using the Cauchy type integral for the determination of $L^0_-(k)$ we found, in particular, that $L^0_-(k_f) = L_-(k_B) = 0.8177 + 0.4593\mathrm{i}$. In addition, using (80) we deduce

$$0.8177\cos\phi + 0.4593\sin\phi = \frac{1}{\mathscr{A}} = \frac{u_c}{A_0}. \tag{82}$$

The graph $\phi(\mathscr{A})$ versus ϕ is plotted in Fig. 19, where the corresponding dependence for the two-dimensional lattice (the case $M_1 = 0.01, \nu = 2$) is also shown. It appears that for the lattice strip $\mathscr{A}_{\min} = 1.2211$ and $\mathscr{A}_{\max} = 2.1771$. It is a remarkable fact that these values correspond to the previously obtained bounds of the region where the steady-state formulation is valid (compare with Section 8.3).

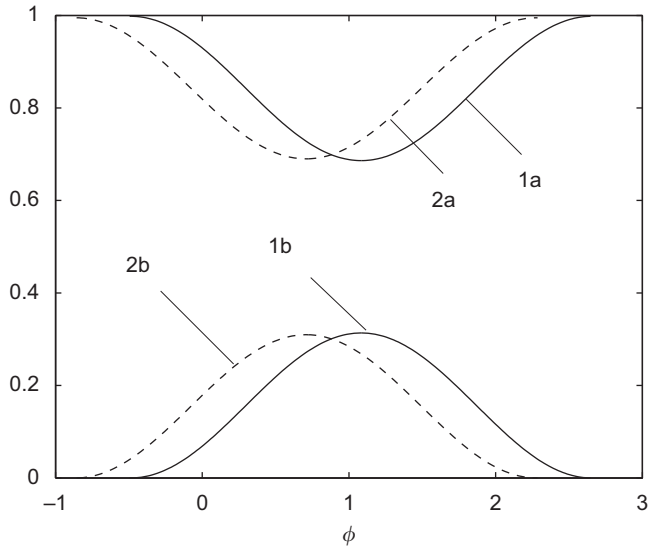

Fig. 20. Energy relations versus the phase ϕ for two cases, $M = 0.01$, $\nu = 2.0$ (1a and 1b) and $M = 0.05$, $\nu = 1.05$ (2a and 2b). The curves correspond to the ratios G_d/G_f (1a and 2a) and G_0/G_f (1b and 2b). The dissipation is minimal at $\phi = 1.0849$ where $G_d/G_f = 0.6861$ (1a) and at $\phi_1 = 0.7076$ where $G_d/G_f = 0.6898$ (1b).

10.4. The energy balance

The energy balance takes the form

$$G_f = G_d + G_r + G_0, \tag{83}$$

where G_f is the energy delivered by the feeding knife wave, $G_d = G_A + G_C$ is the energy radiated via the dissipative waves with the wavenumbers k_A and k_C, G_r is the energy radiated from the interface, and G_0 is the critical strain energy of the bond [see (78) with $U(0) = u_c$]. Note that, for the high-contrast interface the ratio G_r/G_f is very small (see Fig. 18). The ratios G_d/G_f and G_0/G_f are shown in Fig. 20.

11. Discussion

What are the necessary conditions for the existence of the localised wave–fracture configuration? First, the contrast between the interface layer and the surrounding lattice must be sufficiently high, such that the frequencies of the feeding and dissipative waves stay outside the pass band in the dispersion diagram of the uniform lattice. Next, the energy flux in the feeding wave must reach the moving crack front. This implies that the group velocity of the feeding wave propagating from the left, in the crack area, toward the crack front must exceed the crack speed; on the other hand, it must be below the crack speed (it can be positive, zero or negative) if the crack takes energy from the wave placed ahead of the front.

Two well established crack growth regimes were considered, the steady-state regime, $u = u(\eta)$, $\eta = m - \nu t$, and the alternating-strain one, $u = u(\eta)(-1)^m$. Note that propagating feeding and dissipative waves exist in both regimes. The difference lies in the wave phases corresponding to the breakage of the bonds. If in the steady-state regime the bonds break at the feeding wave phase ϕ, then in the alternating-strain regime they break at ϕ for even values of m and at $\phi + \pi$ for odd m (or vice versa). Clearly, the alternating-strain fracture criterion, $|u| = u_c$, is weaker than that for the steady-state regime, $u = u_c$, and hence the corresponding crack speed for the alternating-strain regime should not be less than the steady-state regime speed.

In the formulations adopted in this paper, only the crack-path bonds were allowed to be broken. Of course, due to the symmetry (the displacement field is antisymmetric) these bonds are the first candidates for fracture. However, especially for large amplitudes, the other bonds may break too. To preserve the formulation (and to preserve the localised wave–fracture scenario), at least for large amplitudes, we have to assume that the crack-path interface bonds are weaker enough comparative to the other bonds.

In the above discussed numerical simulations (see Figs. 8–13), along with the steady-state regime we have also observed a crack propagation with a local oscillation of the crack speed. For a sufficiently large amplitude of the feeding wave (the range up to $\mathscr{A} = 100$ was analysed), the averaged (macrolevel) crack speed is established. For a certain range of values of $\mathscr{A}$

it corresponds to the steady-state or alternating-strain regimes, which agrees with the theoretical predictions. At higher amplitudes the established crack speed becomes larger (but still it is less than the feeding wave group velocity). On the other hand, the 'local' speeds, representing the time-intervals between the breakages of neighbouring bonds, appear to alternate between two or more values, one of which corresponds to the locally ordered crack growth.

In conclusion, we note that the lattice considered in this paper can be treated as a model of a structural waveguide. In this regard, the results obtained here can be used in modelling of dynamic fracture of the waveguide under an action of a transmitted wave.

Acknowledgements

The research project was supported by a Marie Curie Transfer of Knowledge Grant of the European Community Sixth Framework Programme under contract number (MTKD-CT-2004-509809). The paper has been completed during the Marie Curie Fellowship of L.I. Slepyan at the University of Liverpool. Provision of academic facilities by the Department of Mathematical Sciences of the University of Liverpool is gratefully acknowledged. We would like to thank the referees for valuable comments and suggestions on the text of the manuscript.

References

Abraham, F.F., Gao, H., 2000. How fast can cracks propagate?. Phys. Rev. Lett. 84 (14), 3113–3116.
Broberg, K.B., 1999. Cracks and Fracture. Academic Press, London.
Burridge, R., 1976. An influence function for the intensity factor in tensile fracture. Int. J. Eng. Sci. 14, 725–734.
Coker, D., Lykotrafits, G., Needleman, A., Rosakis, A.J., 2005. Frictional sliding models along an interface between identical elastic plates subsect to shear impact loading. J. Mech. Phys. Solids 53, 884–922.
Edagawa, K., Suzuki, T., Takeuchi, S., 1977. Motion of a screw dislocation in a two-dimensional Peierls potential. Phys. Rev. B 55 (10), 6180–6187.
Freund, L.B., 1979. The mechanics of dynamic shear crack propagation. J. Geophys. Res. 84, 2199–2209.
Gao, H., Huan, Y., Gumbsch, P., Rosakis, A.J., 1999. On radiation-free transonic motion of cracks and dislocations. J. Mech. Phys. Solids 47, 1941–1961.
Gerde, E., Marder, M., 2001. Friction and fracture. Nature 413, 285–288.
Marder, M., 2006. Supersonic rupture of rubber. J. Mech. Phys. Solids 54, 491–532.
Mishuris, G.S., Movchan, A.B., Slepyan, L.I., 2007. Waves and fracture in an inhomogeneous lattice structure. Waves Random Complex Media 17, 409–428 10.1080/17455030701459910.
Mishuris, G.S., Movchan, A.B., Slepyan, L.I., 2008a. Dynamics of a bridged crack in a discrete lattice. The Quarterly Journal of Mechanics and Applied Mathematics 61 (2), 151–160.
Mishuris, G.S., Movchan, A.B., Slepyan, L.I., 2008b. Dynamical extraction of a single chain from a discrete lattice. J. Mech. Phys. Solids 56/2, 487–495 10.1016/j.jmps.2007.05.020 〈http://dx.doi.org/10.1016/j.jmps.2007.05.020〉.
Movchan, A.B., Bullough, R., Willis, J.R., 2003. Two-dimensional lattice models of the Peierls type. Philos. Mag. 83 (5), 569–587.
Needleman, A., Rosakis, A.J., 1999. The effect of bond strength and loading rate on the conditions governing the attainment of intersonic crack growth along interfaces. J. Mech. Phys. Solids 47, 2411–2449.
Rosakis, A.J., Samudrala, O., Singh, R.P., Shukla, A., 1998. Intersonic crack propagation in bimaterial systems. J. Mech. Phys. Solids 46, 1789–1813.
Rosakis, A.J., Samudrala, O., Coker, D., 1999. Crack faster than the shear wave speed. Science 284, 1337–1340.
Slepyan, L.I., 1981. Crack propagation in high frequency lattice vibrations. Sov. Phys. Dokl. 26, 900–902.
Slepyan, L.I., 2002. Models and Phenomena in Fracture Mechanics. Springer, Berlin.
Slepyan, L.I., Fishkov, A.L., 1981. The problem of the propagation of a cut at transonic velocity. Sov. Phys. Dokl. 26 (6), 1192–1193.